MARS PHOTOCHEMISTRY: WEAK POINTS AND SEARCH FOR SOLUTIONS. Vladimir A. Krasnopolsky, Catholic University of America, Department of Physics, 200 Hannan Hall, Washington, D.C. 20064 (vkrasn@verizonmail.com).

Photochemical modeling is a powerful tool to study the chemical composition of a planetary atmosphere. Using densities of just two or three species near the surface of a planet, photochemistry makes it possible to calculate vertical density profiles for a few dozen species and describe chemical and physical processes that determine these profiles.

Weaknesses of the Current Models of Mars Photochemistry: The latest models of Mars photochemistry [1-5] were made a decade ago. There is an increasing disagreement between the recent experimental data and those models:

1) The standard gas-phase chemistry predicts too low abundances of CO and ozone;

2) All modifications in gas-phase chemistry suggested to agree the models with the observations have not been confirmed;

3) Recent measurements [6, 7] give even greater CO abundance than that in the modified models;

4) The detected H_2 abundance [8] is far below the model predictions;

5) MGS/TES mean H_2O abundance [9] exceeds that used in the models;

6) The observed upper limit to H_2O_2 [10] is smaller than the model predictions by an order of magnitude;

7) The observed low latitudinal variations of the $O_2(^1\Delta)$ dayglow at 1.27 μm [11] and ozone [12] disagree with the very strong variations of H_2O [9] and question the basic concept of Mars photochemistry.

These facts show that the current models are inadequate, incomplete, and needs a significant updating.

Global, Local, and General Circulation Models: One-dimensional global-mean model is a traditional tool to solve basic photochemical problems. Eddy diffusion, which is uncertain within a factor of 3, substitutes atmospheric mixing in these models. The models reflect the global-mean values and are especially good for long-living species H_2, O_2, and CO on Mars.

Local models are adjusted to local conditions. The lifetimes of H_2, O_2, and CO are greater than the global atmospheric mixing time, therefore these species cannot be calculated by the local models. These abundances are the basic experimental constraints, and the chemistry adopted in the local models should be tested by the global models on the consistency with the measured H_2, O_2, and CO.

Photochemical GCMs may appear soon, and that will be a significant progress in photochemical modeling. However, there are two restrictions to those models. First, they do not cover atmospheric mixing at the scales, which are smaller than the model grid step. Therefore, these models either underestimate the atmospheric mixing or should adopt small-scale mixing, similar to that in the global and local models.

The second restriction is a very long run for the GCMs even with the simplest chemistry. Therefore, similar to the local models, the mean abundances of H_2, O_2, and CO are adopted by the photochemical GCMs, and their chemistry should be tested by the global models on the consistency with the measured H_2, O_2, and CO. The models considered below are global mean and without nitrogen chemistry. This is

Table 1. Reactions of CO_2-H_2O chemistry on Mars and their rate coefficients

	Reaction	Rate Coefficient
1	$CO_2 + h\nu \rightarrow CO + O$	-
2	$CO_2 + h\nu \rightarrow CO + O(^1D)$	-
3	$O_2 + h\nu \rightarrow O + O$	-
4	$O_2 + h\nu \rightarrow O + O(^1D)$	-
5	$H_2O + h\nu \rightarrow H + OH$	-
6	$HO_2 + h\nu \rightarrow OH + O$	1.3×10^{-4}
7	$H_2O_2 + h\nu \rightarrow OH + OH$	2.1×10^{-5}
8	$O_3 + h\nu \rightarrow O_2(^1\Delta) + O(^1D)$	1.7×10^{-3}
9	$O(^1D) + CO_2 \rightarrow O + CO_2$	$7.4\times10^{-11}e^{120/T}$
10	$O(^1D) + H_2O \rightarrow OH + OH$	2.2×10^{-10}
11	$O(^1D) + H_2 \rightarrow OH + H$	1.1×10^{-10}
12	$O_2(^1\Delta) + CO_2 \rightarrow O_2 + CO_2$	10^{-20}
13	$O_2(^1\Delta) \rightarrow O_2 + h\nu$	2.24×10^{-4}
14	$O + CO + CO_2 \rightarrow CO_2 + CO_2$	$2.2\times10^{-33}e^{-1780/T}$
15	$O + O + CO_2 \rightarrow O_2 + CO_2$	$1.2\times10^{-32}(300/T)^2$
16	$O + O_2 + CO_2 \rightarrow O_3 + CO_2$	$1.3\times10^{-33}(300/T)^{2.4}$
17	$H + O_2 + CO_2 \rightarrow HO_2 + CO_2$	$1.7\times10^{-31}(300/T)^{1.6}$
18	$O + HO_2 \rightarrow OH + O_2$	$3\times10^{-11}e^{200/T}$
19	$O + OH \rightarrow O_2 + H$	$2.2\times10^{-11}e^{120/T}$
20	$CO + OH \rightarrow CO_2 + H$	1.5×10^{-13}
21	$H + O_3 \rightarrow OH + O_2$	$1.4\times10^{-10}e^{-470/T}$
22	$H + HO_2 \rightarrow OH + OH$	7.3×10^{-11}
23	$H + HO_2 \rightarrow H_2 + O_2$	$1.3\times10^{-11}(T/300)^{0.5}e^{-230/T}$
24	$H + HO_2 \rightarrow H_2O + O$	1.6×10^{-12}
25	$OH + HO_2 \rightarrow H_2O + O_2$	$4.8\times10^{-11}e^{250/T}$
26	$HO_2 + HO_2 \rightarrow H_2O_2 + O_2$	$3.2\times10^{-13}e^{580/T}$
27	$OH + H_2O_2 \rightarrow HO_2 + H_2O$	$2.9\times10^{-13}e^{-160/T}$
28	$OH + H_2 \rightarrow H_2O + H$	$3.3\times10^{-13}(T/300)^{2.7}e^{-1150/T}$
29	$O + O_3 \rightarrow O_2 + O_2$	$8\times10^{-12}e^{-2060/T}$
30	$OH + O_3 \rightarrow HO_2 + O_2$	$1.5\times10^{-12}e^{-880/T}$

Photolysis rates and k_{13} are in s^{-1}, second and third order reaction rate coefficients are in $cm^3\ s^{-1}$ and $cm^6\ s^{-1}$, respectively. Photolysis rates for all species except CO_2, O_2, and H_2O refer to the lower atmosphere, are calculated for $\lambda > 200$ nm and scaled to half values at 1.517 AU.

the case when

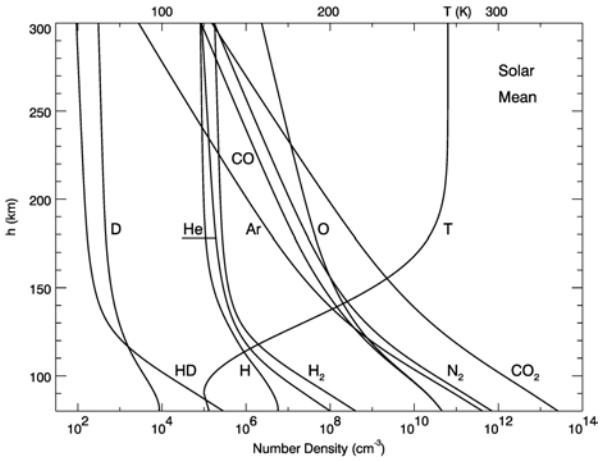

Figure 1. Model of Mars upper atmosphere at medium solar activity [13].

the production of N in the lower thermosphere exceeds the production of NO [1].

Mars Model Upper Atmosphere and Ionosphere: A detailed model for the upper atmosphere and ionosphere of Mars was recently developed [13]. This model includes 11 neutral (Figure 1) and 18 ion species (Figure 2), 32 photon and photoelectron dissociation, ionization, and dissociative ionization processes, and 54 reactions. Both thermal and nonthermal escape processes were considered at the upper boundary of 300 km. Therefore, our current model will cover the altitudes below 80 km, and we will apply the fluxes of H and H_2 at medium solar activity from that model at our upper boundary of 80 km.

Boundary Conditions, Input Data, and Chemical Reactions: The escape of H and H_2 should be perfectly balanced by the escape and/or loss of oxygen for the surface oxidation in the steady-state models of Mars photochemistry. The models diverge if this rule is broken. It does not matter for the model if oxygen escapes or is lost at the surface, and we assume the former.

The hydrogen escape flux and the H and H_2 velocities at the upper boundary were the input data in the previous models [3, 4]. A flux to velocity ratio is density, and we assign the H and H_2 fluxes and the H_2 density from [13] at 80 km in our model. Other boundary conditions reflect the CO_2 dissociation of 1.4×10^{11} cm^{-2} s^{-1} above 80 km and the O_2 dissociation velocity of 0.16 cm s^{-1} at 80 km. Conditions at the lower boundary correspond to the chemically passive surface.

The MGS/TES data on the day- and nighttime temperature structure of Mars atmosphere at L_S = 0, 90, 180, and 270° were properly averaged to get a mean temperature profile. The global-mean water abundance of 15 precipitable μm from the MGS/TES observations [9] results in the H_2O mixing ratio of 260 ppm up to a condensation level at 18 km.

Table 1 presents a standard set of gas-phase reactions for the CO_2-H_2O chemistry on Mars. The reaction rate coefficients are taken mostly from the JPL compilations [14, 15] and some later publications. The photolysis rates have been calculated using the appropriate cross sections from the JPL compilations as well.

Table 2. Some Results of Modeling

Value	Obs	M1	M2	M3	M4
$O_2(\times10^{-3})$	1.2	1.4	1.5	1.3	2.4
CO (0 km, $\times10^{-4}$)	8	0.8	1.0	0.9	2.4
CO (40 km, $\times10^{-4}$)	-	1.5	1.1	1.2	2.6
CO (80 km, $\times10^{-4}$)	-	66	7.6	7.7	9.1
O_3 (μm-atm)	1.5-3	0.63	0.66	0.52	2.6
$4\pi I_{1.27\ \mu m}$ (MR)	≈4	1.14	1.26	1.04	3.8
H_2O_2 (ppb)	<4	20.2	21.3	23.8	3.1

See text for explanation.

Results: Some results of modeling are shown in Table 2. The second column (Obs) gives the observed values. $4\pi I_{1.27\ \mu m}$ (MR) is the $O_2(^1\Delta)$ 1.27 μm dayglow brightness in megarayleighs. Models M1-M3 are for pure gas-phase chemistry with different eddy diffusion coefficient K. K is equal to 10^6 cm^2 s^{-1} for M1, and the abundance of CO near the surface, O_3, and the O_2 dayglow are much below the observed values, while H_2O_2 is far above the upper limit. The CO mixing ratio is greater at 40 km than that near the surface by a factor of 2. If CO were equal to the observed value near the surface, that would occur for K = 10^5 cm^2 s^{-1}. CO is very abundant at 80 km because of the low eddy diffusion.

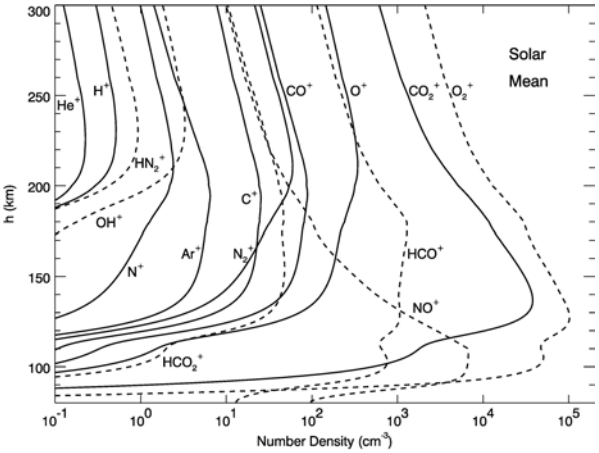

Figure 2. Model of Mars ionosphere at medium solar activity [13].

M2 is for K = 10^7 cm^2 s^{-1}, and it is similar to M1 in many aspects. The difference between M1 and M2 in H_2O_2 is small. This difference was a factor of 2 in the local model [10], maybe, because the H_2, O_2, and CO abundances were fixed in that model. M3 is a model for K increasing from 10^5 near the surface to 10^7 at 40 km and higher [3]. This profile of K is preferable.

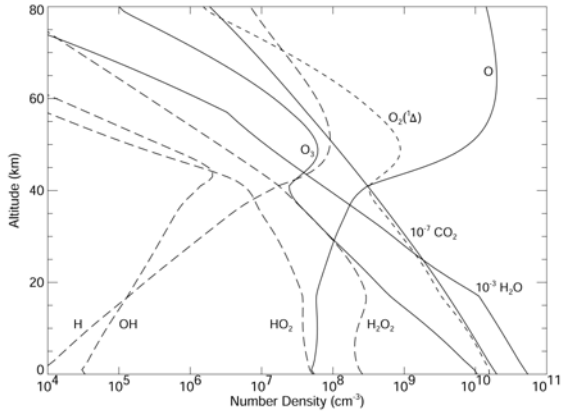

Figure 3. Model for Mars photochemistry (M4) with a heterogeneous sink of peroxide on ice and ice-covered aerosol particles.

All pure gas-phase chemistry models significantly disagree with the observations. However, laboratory data and studies of chemistry of the Earth's atmosphere show that ice particles are very effective in scavenging of all forms of odd hydrogen. Their sticking coefficients may be as high as 1, 0.2, 0.5, and 0.03 for OH, HO_2, H_2O_2, and H, respectively [14, 15].

According to the MGS/TES observations [16], the mean optical depth of ice aerosol is ≈0.05 at 12 μm and ≈0.1 in the visible at 2 p.m., i.e., near the diurnal minimum. Ice may cover some dust particles, and we assume that the altitude distribution of ice and ice-covered particles is similar to that of dust, which is taken from [17]. Model M4 is similar to M3 but includes a heterogeneous sink of H_2O_2 on ice with a probability of 0.025. The O_3 and H_2O_2 abundances and the $O_2(^1\Delta)$ dayglow in M4 agree with the observations (Table 2), while CO is between the measured abundance and that from the gas-phase models. It is clear that the inclusion of heterogeneous chemistry provides a distinct possibility to fit all observational constraints. The calculated vertical density profiles for model M4 are shown in Figure 3.

Our simulations show that a major effect of heterogeneous chemistry is produced by the ice aerosol above ≈5 km. This aerosol opacity may be proportional to the H_2O abundance. Then both production and loss of odd hydrogen are proportional to the water vapor abundance. This helps to explain the low latitudinal variations of the $O_2(^1\Delta)$ dayglow and ozone, in spite of the variations of water vapor by more than an order of magnitude.

Conclusions: (1) There are significant contradictions between the latest photochemical models and the observations.

(2) All these contradictions may be removed by the inclusion of heterogeneous chemistry.

(3) Heterogeneous chemistry is very effective in the Earth's atmosphere. It should exist in the Martian atmosphere, and Mars photochemical models are inadequate without heterogeneous chemistry.

Acknowledgements: I am grateful to Mike Smith who kindly offered the MGS/TES temperature data for this work. This work was supported by the Mars Data Analysis Program via grant NAG5-10492.

References: [1] Krasnopolsky V. A. (1993) *Icarus 101,* 313-332. [2] Atreya S. K. and Gu Z. G. (1994) *JGR 99,* 13133-13145. [3] Nair H. et al. (1994) *Icarus 111,* 124-150. [4] Krasnopolsky V. A. (1995) *JGR 100,* 3263-3276. [5] Clancy R. T. and Nair H. (1996) *JGR 101,* 12785-12790. [6] Clancy R. T. et al. (1996) *Icarus 122,* 36-62. [7] Krasnopolsky V. A. (2003) *JGR 108,* E2, 5010. [8] Krasnopolsky V. A. and Feldman P. D. (2001) *Science 294,* 914-917. [9] Smith M. D. (2002) *JGR 107,* E11, 5115. [10] Encrenaz Th. et al. (2002) *A&A 396,* 1037-1044. [11] Krasnopolsky V. A. (2003) *Icarus* (MS I08520). [12] Clancy R. T. et al. (1999) *Icarus 138,* 49-63. [13] Krasnopolsky V. A. (2002) *JGR 107,* E12, 10.29/2001JE001809. [14] DeMore W. B. et al. (1997) *JPL Pub. 97-4.* [15] Sander S. P. et al. (2000) *JPL Pub. 00-3.* [16] Smith M. D. et al. (2001) *GRL 28,* 4263-4266. [17] Korablev O. I. Et al. (1993) *Icarus 102,* 76-87.